



Magnified charge carrier conduction, permittivity, and mesomorphic properties of columnar structure of a room temperature discotic liquid crystalline material due to the dispersion of low concentration ferroelectric nanoparticles

Rahul Uttam ¹, Sandeep Kumar,^{2,3} and Ravindra Dhar ^{1,*}

¹Centre of Material Sciences, University of Allahabad, Prayagraj 211002, India

²Raman Research Institute, C. V. Raman Avenue, Sadashivanagar, Bengaluru 560080, India

³Department of Chemistry, Nitte Meenakshi Institute of Technology, Bengaluru 560064, India



(Received 4 August 2020; revised 10 September 2020; accepted 6 November 2020; published 30 November 2020)

Liquid crystal nanocomposites have been a hot topic of research due to optimization of physical properties with such blending. There are several reports on enhancement of physical properties of nematic liquid crystals due to the blending of the nanomaterials. L. M. Lopatina and J. V. Selinger [*Phys. Rev. Lett.* **102**, 197802 (2009)] have even proposed a theory based on experimental results for the enhancement of the properties of the nematic mesophase in the presence of ferroelectric nanoparticles. However, discotic liquid crystal nanocomposites are less studied. In the present experimental work, we have studied the effect of ferroelectric (BaTiO₃) nanoparticles on a room temperature discotic liquid crystalline material, namely 1,5-dihydroxy-2,3,6,7-tetrakis(3,7-dimethyloctyloxy)-9,10-anthraquinone. We investigated the physical properties of low concentration ferroelectric nanoparticle dispersed discotic columnar structure, using calorimetric, optical, x-ray diffraction, and dielectric spectroscopy tools. Results show that inclusion of ferroelectric nanoparticles in the discotic matrix consolidates the stability of the columnar matrix of the Col_h phase by virtue of their ferroic nature. An enhancement in charge carrier conductivity by several orders of magnitude at ambient conditions has been observed which makes such systems highly appropriate for one-dimensional conductors. Low concentration of BaTiO₃ nanoparticles substantially enhanced permittivity of the system also. A molecular relaxation mode has been observed in the middle frequency range of the dielectric spectra. Enhancement of these important parameters could be possible due to the ferroelectric nature of the dispersed nanoparticles.

DOI: [10.1103/PhysRevE.102.052702](https://doi.org/10.1103/PhysRevE.102.052702)

I. INTRODUCTION

The emergence of nanotechnology has dovetailed with an increased number of various nanostructures having a substantial impact across a discrete range of fields like energy, medicine, catalysis, optoelectronics, and sensing [1–5]. Nanocomposites based on organic substances, such as liquid crystals with dispersions of ultrasmall inorganic particles, depict suitable models for the study of interphase interactions and determination of the mechanisms of the effect of nanoparticles (NPs) on the characteristic properties of organic matrices [6]. These nanocomposites show improved properties as compared to the pure liquid crystals, resulting in new perspectives for applications in different domains [7,8]. For instance, inclusion of ferroelectric nanoparticles in a liquid crystal matrix significantly enhances its orientational order and electro-optical response, thus reducing the orientational threshold voltage [9–13].

Liquid crystal (LC) compounds represent a certain class of organic molecules showing an intermediate state between crystalline solids and amorphous liquids. Micellar solutions of surfactants, main and side chain polymers, and a large number of biological systems also belong to LCs. A typical LC molecule consists of a central rigid core, known as the mesogen, and another part formed by flexible side chains

known as the spacer. The LC compounds are characterized by long-range orientational order and sometimes one- or two- or even three-dimensional long-range translational or positional order. They exhibit very specific electro-optical phenomena, not found in solids or liquids. It is possible to tune the electro-optical properties of LC compounds only by altering the LC molecule's orientation. This feature is useful in display applications, thermometers, high modulus fibers, and optoelectronic devices [14].

The combined effect of LCs and nanoparticles is twofold. LCs act as a smart solvent for the nanomaterials providing them long-range, self-alignment structure and manipulation by the use of external fields. Similarly, the nanomaterials can tune the physical properties of LCs due to the similarity of the dimensions [15]. A LC-nanomaterial composite system is prepared to (i) modify the primary physical or chemical properties of the pristine LCs [16–18], (ii) manipulate and order nanomaterials in LCs to modify the properties of nanomaterials [19], and (iii) obtain additional functionalities that are available from neither the LCs nor the nanomaterials in their intrinsic states [20]. Dilute nanosuspensions are usually prepared as these are stable due to the weak interactions of the nanoentities at lower concentrations. Nanoentities are small enough to retain the ordering of LC molecules so that macroscopically identical structures are obtained. On the other hand, particles are large enough to retain their intrinsic properties and share these properties with the LC materials [21].

*Corresponding author: dr_ravindra_dhar@hotmail.com

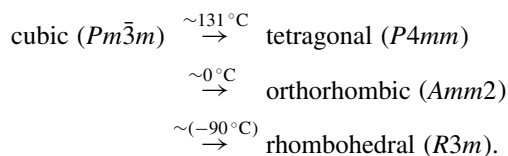
During the past few years, emphasis was on the study of discotic liquid crystal nanocomposite systems [12,22,23]. Discotic liquid crystals (DLCs) are unique nanostructures with exceptional optoelectronic properties. The self-assembly of appropriately functionalized disklike molecules prompts the formation of mesophasic structures [12,15]. Generally, these materials consist of flat or nearly flat central aromatic disk-shaped cores, substituted by more than three flexible aliphatic carbon chains. Such functionalized disk-shaped molecules spontaneously self-assemble into nematic, columnar, or lamellar mesophases [22,23]. This is a dynamic state of ordered molecular aggregation. The least-ordered, most-mobile mesophase is the discotic nematic (N_D) phase. In this phase, molecules possess only orientational order with no long-range positional order. As a result of the strong tendency of aromatic molecules to aggregate face-to-face, the majority of DLCs (approximately 95%) form columnar phases in which molecular disks stack one on top of the other to form a column, similar to a pile of coins. These columns of disks can then self-organize into different lattices, for example, a hexagonal lattice (Col_h), rectangular lattice (Col_r), and oblique lattice (Col_{ob}). DLCs with large π -conjugated aromatic rings enhance the columnar stability, supramolecular order, and high charge carrier mobility due to extended π -orbital overlap. The mesophases formed by discotic molecules are extremely important from device application perspectives. Among nanoparticles (NPs), plasmonic NPs have been the center of research because of their attractive properties, such as behavior of individual particles and (quantum) size-related electronic, magnetic, and optical effects [24]. Kumar *et al.* reported a 250 times enhancement in the value of conductivity due to the dispersion of gold nanoparticles in a discotic matrix of HHTT [25]. Similarly, Holt *et al.* reported a 6 order of magnitude enhancement in conductivity due to doping of functionalized gold nanoparticles in the discotic matrix [26].

The 1,2,3,5,6,7-hexahydroxy-9,10-anthraquinone, also known as rufigallol, is known to act as a core fragment in a variety of discotic liquid crystals (DLCs). Rufigallol-based DLCs are fascinating in nature as these molecules have an elongated core with a twofold symmetry axis [22,25]. Rufigallol derivatives are one of the earliest discovered systems reported to form columnar mesophases. Shape anisotropy, microsegregation between flexible chains and rigid cores, and core-core van der Waals attractions are postulated to be the driving force for the formation of columnar mesophases. The core in rufigallol is electron deficient in nature [25]. Furthermore, because of their liquid character, they possess the capacity to self-heal structural defects such as grain boundaries. The self-organization of discotic mesogenic molecules into the various liquid-crystalline phases is driven by the anisotropy in the intermolecular interactions (mainly steric and dispersion interactions) between the highly anisometric molecules [22,25]. The self-assembly of disk-shaped molecules results in one-dimensional columns, and these columns in turn form two-dimensional hexagonal lattices, well insulated from neighboring columns by insulating alkyl chains attached to the core [22,25]. The columnar hexagonal phase, exhibited by most of the rufigallol derivatives, has strong anisotropic electronic transport properties that are

conjugated to unidirectional intermolecular coupling along the column axis. Polymorphism, high diffusion lengths, thermal stability, and color make them promising candidates for applications in molecular electronics and high efficiency photoconductive switches, solar cells, and organic light emitting diodes. However, the conductivity of these LCs is low. Doping them with suitable nanoentities may help in increasing their conductivity and making them more worthy for use in technological applications [26].

Through the above discussion, it seems that ferroelectric nanoparticles (FNPs) do modify the physical properties of LC matrixes, leading to an improvement in the electro-optic performance. However, due to the complicated size-dependent ferroelectricity and aggregation behavior of ferroelectric nanoparticles in LCs, additional research is necessary. These DLC+FNP composites may potentially possess versatile applications in electronic and optical nano-devices as they provide a new opportunity to tune the properties of liquid crystals without going into the complex process of chemical synthesis [27,28].

In the present study, we incorporated barium titanate nanoparticles (BTNPs) in the discotic matrix. We have used 1,5-dihydroxy-2,3,6,7-tetrakis(3,7-dimethyloctyloxy)-9,10-anthraquinone (RTAQ) as a host to BTNPs. Earlier, Yadav *et al.* have dispersed CdSe quantum dots in RTAQ [28] and found substantial ($\sim 10^\circ\text{C}$) decrease of mesophase transition temperatures. Thus our aim is to see whether FNPs give results other ways as in the case of FNP-nematic liquid crystal systems [10]. Barium titanate, BaTiO_3 (BT), is the first polycrystalline ceramic material discovered that exhibited ferroelectricity. BaTiO_3 has isotropic polyhedron particle shapes. At room temperature, BaTiO_3 single crystals exhibit tetragonal crystal structure with [001] polar axis and a spontaneous polarization of $26 \mu\text{C}/\text{cm}^2$. The dielectric constant of the BaTiO_3 single crystal is 168, in the direction parallel to the polar axis, and 2920, perpendicular to the polar axis [29,30]. BT based materials are quite versatile for fundamental studies since their functional properties are sensitive to both microstructure and chemical modifications. Experiments have shown that BTNPs at low concentrations ($<1\%$) enhance the physical properties of liquid crystals by coupling with the orientational ordering of the macroscopic medium [10,21]. Li *et al.* have suggested that these nanoparticles produce large local electric fields, which polarize the LC molecules and hence increase the intermolecular interaction between the host-dopant molecules [21]. The phase transitions in BaTiO_3 crystal are of martensitic type, primarily due to the change in the polarization dependent crystalline anisotropy energy [31,32]. In the martensitic phase transitions, the atoms (or the ions) change their positions and the diffusional movements of the atoms (or the ions) are not involved. For BaTiO_3 single crystals, the experimental observations have demonstrated the sequence of first order phase transitions as follows [31,32]:



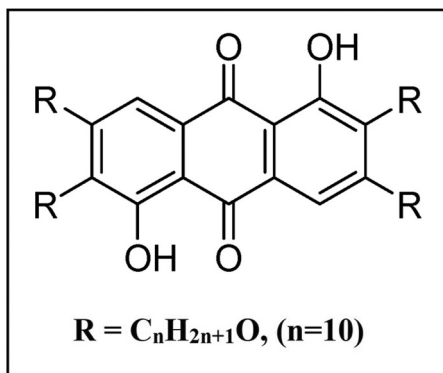


FIG. 1. Molecular structure of 1,5-dihydroxy-2,3,6,7-tetrakis(3,7-dimethyloctyloxy)-9,10-anthraquinone (RTAQ).

II. EXPERIMENTAL DETAILS

Figure 1 shows the molecular structure of the host DLC, RTAQ. This has the widest columnar hexagonal room temperature mesophase. RTAQ is a difunctional molecule, with two aromatic rings, two carbonyl groups, and four ether groups linked together. The RTAQ molecule was synthesized in the same way as reported earlier by Bisoyi *et al.* [33]. It is deep orange in color and shows columnar hexagonal phase, confirmed by x-ray diffraction as well as texture studies. The BTNPs (size $\lesssim 50$ nm, purity $\geq 99\%$) procured from Sigma-Aldrich has been used in the present study. The literature suggests that for BTNPs, the critical size below which the ferroelectric nature vanishes is ~ 10 nm [13,34–37]. Li *et al.* suggested that the optimal range for the particles to directly influence the system molecules without disturbing the director field is 10–100 nm [21]. Earlier, we reported results on 0.5 and 1.0 wt.% of BTNPs in RTAQ and concluded that further lowering of BTNPs may yield better results [38]. Accordingly, we complemented the study by doping 0.15 wt.% of BTNPs in RTAQ. Taking radius of BTNPs ~ 25 nm, density ~ 5.85 g cm $^{-3}$, molecular weight of RTAQ = 865 g mol $^{-1}$, and Avogadro's number as 6.022×10^{23} mol $^{-1}$, 0.15 wt.% of BTNPs in RTAQ translates into 1 BTNP against approximately 0.18 million RTAQ molecules. The LC-NP composites were prepared by adding a small weight percentage of BTNPs in the discotic LCs. Shimadzu's semimicro balance (AUW120D) having an accuracy of 10 μ g was used for weighing. The DLC was dissolved in chloroform and ultrasonicated with BTNPs for 2 hours to obtain uniform mixture, and slow evaporation of the solvent resulted in the formation of the nanocomposite. Doping was done at lower concentration to minimize chances of immiscibility and aggregation, which is important for obtaining good results [15]. Figure 2 is the schematic representation showing how the NPs may get accommodated inside the DLC matrix, in both the isotropic liquid (I) phase and discotic columnar hexagonal (Col $_h$) phase.

The composites were characterized using a polarizing optical microscope (POM), small-angle x-ray scattering (SAXS), a differential scanning calorimeter (DSC), and dielectric spectroscopy. Before taking the composite for different measurements, these were once again mixed in its isotropic liquid phase (for about 30 minutes) by using a magnetic stirrer.

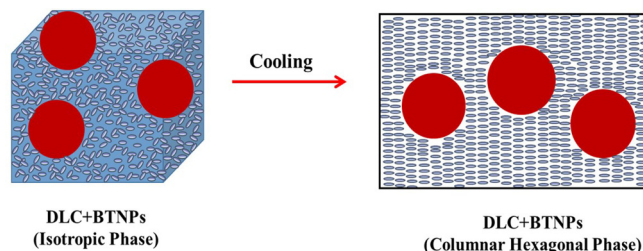


FIG. 2. Schematic indicative illustration displaying FNPs inside the DLC in I and Col $_h$ phase. Actual dimensional ratio of BTNPs and DLC molecules is approximately 17 to 1. Precise alignment of discotic molecules in the vicinity of FNPs will be discussed later in the Results and Discussion section.

The transition temperature and associated transition enthalpy/entropy values for the mesophase transitions were determined using DSCs of NETZSCH (model DSC-200-F3-Maia) and TA Instruments (model DSC Q20), which were operated at different scan rates of 15.0, 12.5, 10.0, 7.5, 5.0, 2.5 $^{\circ}$ C/min. A DSC was allowed to run initially for the first two cycles with the scan rate (SR) of 5 $^{\circ}$ C/min in the range -30 $^{\circ}$ C to 130 $^{\circ}$ C in order to stabilize the transition temperatures and corresponding enthalpy of composites. The textural observations of the mesophase (at a magnification of up to 100 \times) were carried out by using a POM coupled with a heating stage (Instec model HS-1) joined with the temperature controller (Instec model mK 2). The sample was heated to the isotropic liquid phase and slowly cooled at the rate of 0.1 $^{\circ}$ C/min for recording optical textures. The SAXS study was carried out in sealed Lindemann capillary tubes (0.7 mm diameter) using Cu- $K\alpha$ ($\lambda = 1.54$ \AA) radiation from a Rigaku UltraX 18 rotating anode generator with a graphite crystal diffractometer operating at 50 kV and 80 mA current. BTNP XRD spectra (Fig. 3) were analyzed by using Cu- $K\alpha$ ($\lambda = 1.54$ \AA) radiation from a Rigaku SmartLab SE, automated multipurpose x-ray diffractometer equipped with a theta-theta goniometer, operating at 40 kV and 50 mA current. Observed spectra match well with the JCPDS card No. 31-0174 and COD card No. 1522129 for

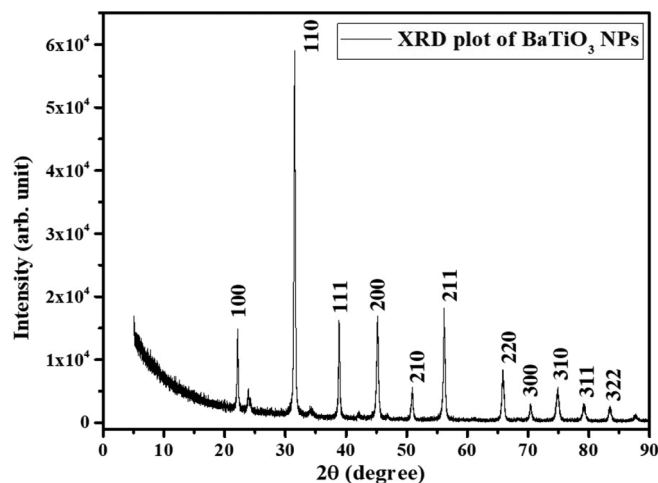


FIG. 3. X-ray diffraction spectra of barium titanate nanoparticles.

BTNPs. The estimated size of BTNPs comes out to be ~ 40 nm by using the Scherrer equation for the most intense peak at 22.1° . Dielectric measurements were carried out using an impedance analyzer (Novocontrol Alpha-A High Performance Frequency Analyzer) in the frequency range 1 Hz to 40 MHz. Temperature of the sample was controlled with the help of a hot stage (Instec model HCS 302) joined with the temperature controller (Instec model mK 1000). The dielectric study of the sample was carried out under homeotropic geometry wherein the plane of discotic molecules is parallel to the electrode's surface. The sandwiched type (capacitors) cells were made using two glass substrates coated with indium tin oxide (ITO) layers. The thickness of the cell was defined by placing two Mylar spacers (thickness $10\ \mu\text{m}$) between the glass plates. These cells have been used for the optical textures studies as well. The sample was introduced via capillary action by heating the sample to the isotropic liquid phase. In order to achieve homeotropic alignment, the sample was slowly cooled at the rate of $0.1\ ^\circ\text{C}/\text{min}$ from the isotropic phase. This usually adopted process yields reasonably good quality of homeotropic alignment due to minimum energy configuration of discotic molecules. The sample temperature was determined by measuring the thermo emf of a copper-constantan thermocouple with the help of a six and half digit multimeter (Agilent model-34410A) with the accuracy of $\pm 0.1\ ^\circ\text{C}$. A measuring electric field of magnitude $0.5\ \text{V}_{\text{rms}}$ was applied normal to electrode surfaces while acquiring the electrical data. Dielectric isotherm spectra were recorded at $0.5\ ^\circ\text{C}$ intervals. Before each frequency scan, the temperature was kept constant to within $\sim 0.1\ ^\circ\text{C}$. For calculating the dielectric parameters such as permittivity, loss, and conductivity of the nanocomposites from measured impedance data, the cell was calibrated by filling standard nonpolar liquid (cyclohexane) in the cell. This gives the active capacitance of the dielectric cell in use. Complete removal of the cyclohexane was ensured before and after filling the liquid.

Dielectric spectra were analyzed by using the generalized Cole-Cole equation [39–41] given here:

$$\begin{aligned} \varepsilon^* = \varepsilon' - j\varepsilon'' = \varepsilon'(\infty) + \sum \frac{(\delta\varepsilon)}{1 + (jf\tau)^{(1-\alpha)}} \\ + \frac{A}{f^n} - j \frac{\sigma_i}{\varepsilon_0\omega^k} - jBf^m. \end{aligned} \quad (1)$$

The real and imaginary parts of Eq. (1) can be written as

$$\begin{aligned} \varepsilon' = \varepsilon'(\infty) + \sum \frac{\delta\varepsilon [1 + (\omega\tau)^{(1-\alpha)} \sin(\frac{\alpha\pi}{2})]}{1 + (f\tau)^{2(1-\alpha)} + 2(f\tau)^{(1-\alpha)} \sin(\frac{\alpha\pi}{2})} \\ + \frac{A}{f^n}, \end{aligned} \quad (2)$$

$$\begin{aligned} \varepsilon'' = \sum \frac{\delta\varepsilon(\omega\tau)^{(1-\alpha)} \cos(\frac{\alpha\pi}{2})}{1 + (f\tau)^{2(1-\alpha)} + 2(f\tau)^{(1-\alpha)} \sin(\frac{\alpha\pi}{2})} \\ + \frac{\sigma_i}{\varepsilon_0\omega^k} + Bf^m, \end{aligned} \quad (3)$$

where $\delta\varepsilon [= \varepsilon'(0) - \varepsilon'(\infty)]$, $\tau (= 1/f)$, and α are dielectric strength, relaxation time, and the distribution parameter ($0 \leq \alpha \leq 1$), respectively. $\varepsilon'(0)$ and $\varepsilon'(\infty)$ are the low and high

frequency limiting value of the relative permittivity. The third and second terms of Eqs. (2) and (3) represent the contribution of electrode polarization capacitance and ionic conductance, respectively, in the low frequency region [40,41]. A , B , k , m , and n are fitting parameters. σ_i is the ionic conductivity. k is usually $\simeq 1$ in the case of dc conductivity. The imaginary part of the permittivity (ε'') may contain a contribution above 100 kHz due to finite resistance of the electrodes and lead inductance [41]. An additional imaginary term Bf^m is empirically added in Eq. (3) to partially account for this effect [41]. The frequency dependence of ε' and ε'' was fitted simultaneously to obtain the dielectric strength and the relaxation frequency, besides the above mentioned parameters. The aim of nonlinear fitting is to estimate the parameter values that best describe the data and minimize the deviations. Here the best fitting is characterized by the value of chi squared (χ^2) and the correlation coefficient (R^2). For the best fitted curve, the value of χ^2 should tend to 0 and the value of R^2 should tend to 1. By the process of fitting, the best fit values of various parameters of Eqs. (2) and (3) were obtained. Low and high frequency correction terms were calculated with the obtained fitting parameters. These terms were then subtracted from the measured data to get the correct dielectric data, free from low and high frequency parasitic effects [40,41]. By substituting fitting parameters in Eqs. (2) and (3) or excluding low and high frequency correction terms from the measured data, error free dielectric data can be generated.

III. RESULTS AND DISCUSSION

A. Thermodynamic study

Characterization of LC compounds specifies the phase as well as the intermolecular interactions between LC molecules. The differential scanning calorimetry (DSC) technique complements the optical methods for determining the phase transitions [14]. DSC measurements were performed in the temperature range $-20\ ^\circ\text{C}$ to $125\ ^\circ\text{C}$ under inert conditions to analyze the stability of LC phases and possible effects induced by the dopant. Figure 4 shows the DSC plots taken at the scan rate of $5\ ^\circ\text{C}\ \text{min}^{-1}$ in the heating and cooling cycles. Various thermodynamic parameters obtained from the analysis of DSC thermograms are listed in Table I. DSC was operated at different scan rates of 2.5, 5.0, 7.5, 10.0, 12.5, and $15.0\ ^\circ\text{C}\ \text{min}^{-1}$, in the heating and cooling cycles. On heating and cooling the sample, peaks signifying columnar hexagonal–isotropic ($\text{Col}_h\text{-I}$) and isotropic–columnar hexagonal (I-Col_h) transitions appear. As the scan rate increases, the system lags from the condition of thermal equilibrium due to thermal inertia of the system, and hence different values for transition temperature (T_p) are obtained for different scan rates. Hence, in order to determine the true transition temperature under thermal equilibrium, we determine the extrapolated T_p at the SR of $0\ ^\circ\text{C}\ \text{min}^{-1}$. Transitions temperatures thus obtained show negligible hysteresis effect between heating and cooling cycles [42]. The extrapolated values of T_p are given in Table I.

Most often, inclusion of NPs in the LC matrix leads to the decrease of mesophase transition temperatures. This is because of the effect of dilution suggested by Gorkunov

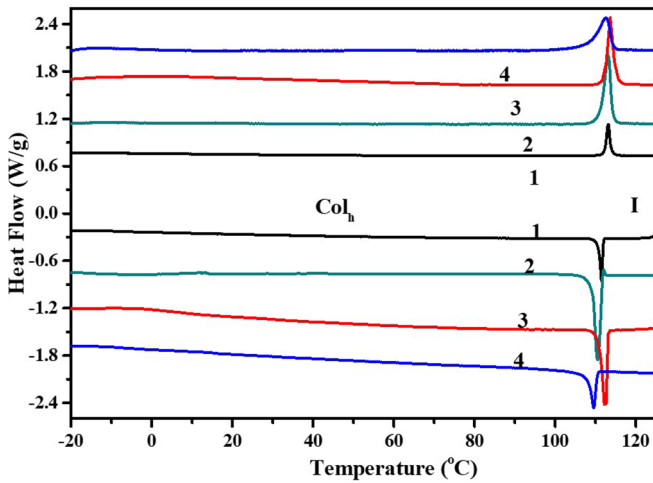


FIG. 4. DSC thermograms during heating and cooling cycles at the scan rate of 5.0 °C/min for (1) RTAQ, (2) RTAQ + 0.15 wt.% BTNPs, (3) RTAQ + 0.5 wt.% BTNPs, and (4) RTAQ + 1.0 wt.% BTNPs.

and Osipov mean field theory for liquid crystal–nanoparticle composites [43]. According to the theory, NPs decrease the ordering (mathematically, order parameter S) in the nanocomposite systems by lessening the interaction between the liquid crystal molecules. Similar results were found in previous studies as well [28,36]. Yadav *et al.* dispersed CdSe quantum dots in RTAQ [28] and found substantial (~ 2 – 12 °C) decrease of $I \leftrightarrow \text{Col}_h$ transition temperatures. Such results are expected because insertion of NPs in columns and domain boundaries disturbs the packing of molecules and hence ordering is reduced. However, in our present studies, $I \leftrightarrow \text{Col}_h$ transition temperature has increased (by 0.5 °C) for 0.5 wt.% BTNPs in RTAQ but decreased (by 1.7 °C) for 1.0 wt.% BTNPs in RTAQ. Thus the presence of BTNPs in RTAQ has in fact improved the $I \leftrightarrow \text{Col}_h$ transition temperature by 3–10 °C in comparison to similar system of CdSe quantum dots in RTAQ. This is due to the ferroelectric nature of BTNPs as observed by Lopatina *et al.* [10] and others in the case of NLC-BTNP systems [21,44].

In fact the effect of FNPs on the mesophase behavior can be explained by considering two types of interactions. One is decreasing interactions between LC molecules due to the dilution effect as discussed in the previous paragraph and it introduces a decrease in the order parameter say by $-\Delta S_1$.

Clearly such interaction decreases with the increasing concentration of FNPs and hence magnitude of ΔS_1 increases. The other one is the interaction of LC molecules (dipoles) with the electric field of FNPs (see Fig. 5). This interaction is expected to increase with the increasing concentration of FNPs. This second type of interaction supports increase of the order parameter. Let change in the order parameter due to it be ΔS_2 . Thus net change in the order parameter of the mesophase due to the doping of FNPs would be $\Delta S = \Delta S_2 - \Delta S_1$. However, it is well known fact that at higher concentrations, NPs show agglomeration [28,38,44] which prevent increase of such interaction and hence ΔS_2 beyond a certain limit. At certain critical doping concentration two interactions may counter each other resulting in the net effect ΔS being zero. If ΔS is positive then the mesophase is expected to stabilize resulting in an increase in $I \leftrightarrow \text{Col}_h$ transition temperature, whereas if ΔS is negative then the mesophase is expected to destabilize resulting in a decrease in $I \leftrightarrow \text{Col}_h$ transition temperature. We will discuss this second type of interaction in detail in the forthcoming section on dielectric studies.

The $I \leftrightarrow \text{Col}_h$ transition temperature is increasing for composite 2 (112.8 °C) whereas it is decreasing marginally for composite 1 (111.9 °C) but substantially for composite 3 (111.1 °C) in comparison to pure RTAQ (112.3 °C). This is probably because as the concentration of doped molecules is increased, the probability of their agglomeration also increases which tries to disorient the system from their self-linking columnar nature. This strain in the lattice formation is opposed by the ferroic nature of the doped nanoparticles, which affects the neighboring discotic molecules present around them [44]. Hence, a tug of war occurs in between the two constraints and the system shows some signs of improvement when an appreciable number density of nanoparticles is present in the system. But as soon as the concentration of doped nanoparticles is further increased (~ 1.0 wt.%), agglomeration starts and hence the effect of dilution supersedes the interaction between the host-dopant molecules. Similar results were reported in previous studies as well [45–49]. Reznikov *et al.* [50] reported that at higher concentrations of NPs, almost rigid LC suspensions are formed. Similar results were reported in previous studies by our group [15,51].

It has been observed that transition enthalpies and entropies are independent of SR and their average values are given in Table I. On the other hand, width of the transition and peak height decrease almost linearly with decrease of the SR. Like transition temperature, there extrapolated values at the

TABLE I. Thermodynamic parameters, viz., peak transition temperature (T_p in °C at SR = 5 °C/min), average enthalpy (ΔH in J/g) and entropy [ΔS in J/(g K)], extrapolated values of full width (W in °C), peak height (h), and peak transition temperature (T_0 in °C) for RTAQ and composites.

System	Heating cycle (Col_h -I)					Cooling cycle (I- Col_h)					T_0
	ΔH	T_p	$W(T_s \sim T_e)$	h	ΔS	ΔH	T_p	$W(T_s \sim T_e)$	h	ΔS	
RTAQ	5.77	113.2	1.2	0.28	0.0149	5.81	111.5	0.6	0.48	0.0151	112.3
RTAQ + 0.15 wt.% BTNPs	5.73	113.1	2.5	0.24	0.0148	5.65	110.7	1.0	0.88	0.0147	111.9
RTAQ + 0.5 wt.% BTNPs	4.57	113.7	1.4	0.60	0.0118	4.52	111.8	0.5	1.28	0.0118	112.8
RTAQ + 1.0 wt.% BTNPs	5.57	112.5	4.8	0.08	0.0145	5.24	109.7	1.2	0.40	0.0137	111.1

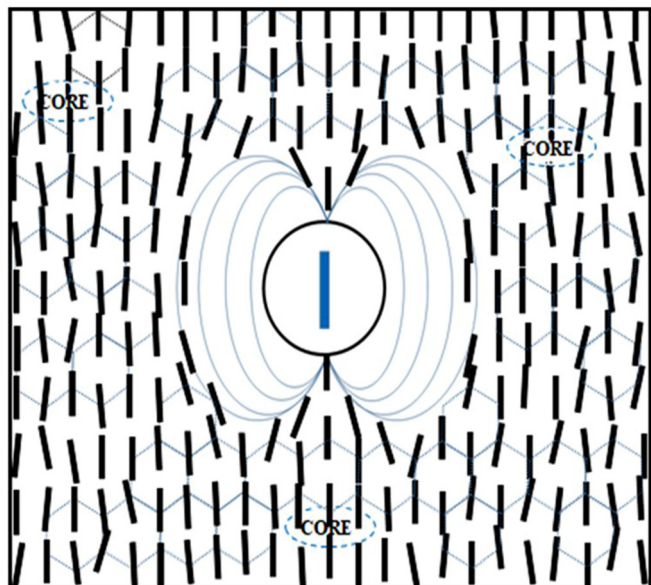


FIG. 5. Schematic illustration displaying ferroelectric nanoparticles as an electric dipole that produces an electric field, and interacts with the molecules to align their column axis (shown by bars) with field. Note that in the Col_h phase, molecular columns lie on the corner of hexagon as shown by light broken lines. Columns are normal to the plane of the molecular disk (core). Away from the FNPs, column axes show fluctuations due to the thermal energy whereas near FNPs, electric field minimizes fluctuations and aligns column axis with the field.

hypothetical SR of 0°C min^{-1} (i.e., under thermal equilibrium) are also listed in Table I. Transition enthalpy, entropy, and width of the transition are minimum whereas height of the peak is maximum for composite 2 suggesting that it has optimum and stable structure. Enhancement in the stability of the mesophases is already reported for FNP-LC systems [10,21,52]. However, this stability tends to decrease in higher concentrations due to agglomeration of nanoparticles. This is primarily because at higher concentrations, due to agglomeration, effective properties of the nanoentities are weakened and hence no enhancement is seen. That is why doping of nanoentities at higher concentrations is usually avoided in the absence of any stabilizing agent.

B. Optical textures study

Polarized optical microscopy (POM) is a standard tool for the identification of liquid crystal phases and determination of phase transitions. However, under POM study, the system is not perfectly isolated with (normal) atmospheric conditions; hence, the transition temperatures obtained from POM are slightly different from those obtained from DSC. Liquid crystals are optically anisotropic in nature, and the director represents the average direction of alignment of molecules. To observe textural variations due to director disorientation (defects), POM is kept under the cross polarizers condition. In DLCs, there are two possibilities to align the disk-shaped molecules. If the disk column axis is in the plane of the bounding surfaces, the alignment is called planar alignment, and

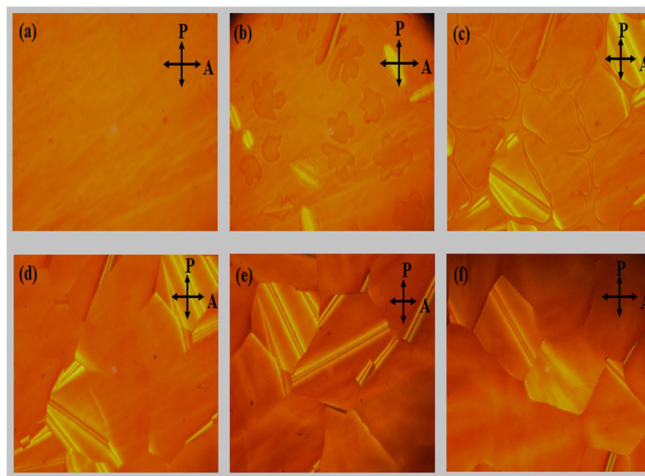


FIG. 6. Optical textures for composite 1 (RTAQ + 0.15 wt.% BTNPs) for (a) isotropic phase (125.0°C), (b) transition state (110.8°C), (c) and (d) cooling down further to Col_h phase at 100.0°C and 75.0°C , respectively, (e) in Col_h phase at room temperature (30.0°C), and (f) at room temperature (after overnight).

when the column axis is perpendicular to the bounding surfaces, it is called homeotropic alignment [53]. In the present case, when the sample was taken in a thin cell of thickness $10\ \mu\text{m}$, homeotropic alignment was obtained on slow cooling ($0.1^\circ\text{C min}^{-1}$) from the isotropic phase.

Optical textures of composite 1 (0.15 wt.% BTNPs in RTAQ) are shown in Fig. 6 during slow cooling ($0.1^\circ\text{C min}^{-1}$) from the isotropic phase. These textures are almost the same as in the case of pure RTAQ [38]. In the isotropic phase, when molecules are randomly oriented, an almost dark uniform texture [Fig. 6(a)] has been observed. However, in the columnar phase [Fig. 6(b)], large domains are formed signifying that columns are trying to align homeotropically (*face-on* orientation) on untreated glass substrates. Some bright domains can also be seen distributed nonuniformly over the field of view. These signify areas where molecular planes may be slightly tilted with respect to the glass substrate. These are π disclinations or defects. The slight variation in background color of nanocomposite is because of dispersion of the NPs. The following analogy can be proposed for the development of pseudo-focal-conic type textures in the pure RTAQ and its nanocomposite. On cooling the samples (both the pure DLCs as well as the nanocomposite), just as transition occurs, heterogeneous nucleation and the growth of non-birefringent hexagonal germs (tiny domains) occurs. These sixfold symmetric domains remain there up to the room temperature. In addition, the lack of birefringence is retained at room temperature, ruling out the assumption of an isotropic liquid state. This optical feature is characteristic of homeotropic alignment, where the column orientation—corresponding to the optical axis of the liquid crystal—coincides with the direction of light propagation, perpendicular to the substrate. Thus, there is no optical anisotropy detectable by polarizing microscopy. Also, the sixfold symmetry of germs is an additional signature of homeotropic alignment of the hexagonal columnar

mesophase. This sixfold symmetry demonstrates the face-on columnar orientation developed over large areas [54,55].

However, it is important to mention that in the case of nanocomposites, alignment does not seem perfect as the intensity of light is higher as compared to that in the pure system. Both the composite and virgin host compose a typical fan-like structure (pseudo-focal-conic type textures) that can be seen at various temperature ranges [56,57]. Generally, POM gives first idea if NPs tend to aggregate in mesophases. In the present DLC-BTNP composite, aggregation of BTNPs is not visible in the columnar phase. As the system cools down from the isotropic phase and the transition point (I-Col_h) is achieved, nonuniform domains are formed throughout the field of view signifying variable alignment of columns. The alignment of columns depends on two factors: first, the core-core interaction, and second, the adhesion/steric repulsion between the alkyl chains attached to the core. As the temperature is further decreased, these domains aggregate to form bigger domains indicating formation of well-aligned columnar structures with respect to the substrate. As evident from the textures, the color and area of the domains change with respect to the decrease in temperature. At room temperature, some divergence in the case of composites from pure RTAQ is visible. For instance, an increased number of π -disclination-like regions is observed in the case of composites. This suggests the decrease in ordering due to impurity addition. The sample kept overnight show slight increase in dark regions which is possibly due to the interaction between the doped molecules which tries to fit well inside the columns and form a stable mesophase. Additionally, RTAQ and its nanocomposite do not show any crystallization down to room temperature.

C. Dielectric study

Dielectric spectroscopy is a powerful method to study the molecular dynamics of collective and noncollective behavior of molecules. Electrical conductivity in the material takes place due to the ordered motion of weakly bound charges under the influence of an electric field. It is one of the significant properties of materials and depends on the nature of charge carriers that dominate the conduction process, such as electrons and holes or cations and anions and their response as a function of temperature and frequency.

1. Frequency and temperature dependent conductivity

In the present studies, when the sample was taken in a thin cell of thickness 10 μm , spontaneous homeotropic alignment (i.e., the plane of disks parallel and column axis perpendicular to the surfaces of the electrodes) was obtained on slow cooling (0.1 $^{\circ}\text{C min}^{-1}$) from I phase. In DLCs, it has been reported that conductivity (σ) improves due to the incorporation of NPs [12,22–23,26,58]. A similar trend was observed in the present study as well due to the inclusion of BTNPs in the columnar matrix. Frequency response of the conductivity is shown in Fig. 7 for pure RTAQ and its nanocomposites. The curves follow the Jonscher's universal power law [59], given as

$$\sigma(f) = \sigma_i + Af^p, \quad (4)$$

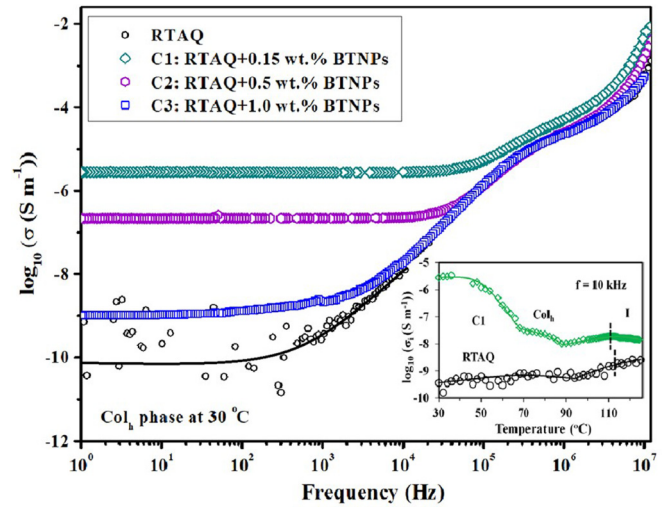


FIG. 7. Frequency dependence of total conductivity (σ) for RTAQ and composites for Col_h phase at 30.0 $^{\circ}\text{C}$. Inset shows variation of ionic conductivity (σ_i) with temperature for RTAQ and composite 1, i.e., 0.15 wt.% of BTNPs in RTAQ. Vertical dashed lines represent I-Col_h transition.

where A is a constant, p is the fraction component, $\sigma(f)$ is the total conductivity, and σ_i is the ionic conductivity of the sample. At low frequencies ($f < 1$ kHz), the second part, i.e., Af^p of the right hand side, is negligible and hence conductivity is composed of only the ionic part [60]. Af^p is the pure dispersive component of ac conductivity having a power law characteristic in terms of frequency f and exponent p ($0 \leq p \leq 1$) that represents the degree of interaction between mobile ions and lattices around them, with A as a constant that determines the strength of polarizability. The following points characterize Fig. 7: (i) A plateau region at low frequencies corresponds to σ_i . In this frequency region, the conductivity, σ_i , increases with increasing temperature. (ii) In the high frequency region, the conductivity is governed by Af^p . Origin of the frequency dependence of conductivity is due to the dipolar relaxation phenomena.

The value of σ_i for pure RTAQ was found to be $10^{-10} \text{ S m}^{-1}$ which is in agreement with the values reported in previous studies [28]. In general, σ_i is high for nanocomposites as compared to pure RTAQ. For composite 1 (i.e., 0.15 wt.% BTNPs in RTAQ), σ_i is highest and it is enhanced by about five orders of magnitude as compared to pure RTAQ. Figure 7 shows that the value of σ_i is high for nanocomposites as compared to pure RTAQ. This establishes the idea of improvement in the hopping charge conductivity due to the presence of impurity ions in the discotic matrix. This is expected because in nanocomposite system, we can assume that the hopping mechanism is favorable along the columns which provide a quasi-one-dimensional path for the charge transport where nanoparticles are covered with a unidirectional pathway kind of system along with discotic molecules. A donor-acceptor-donor-like relation is formed in between highly π electron rich discotics and the ferroic nanoparticles, and hence, generated charges migrate from disk to disk at a larger scale and this is why conductivity shows an enhancement in composites as compared to pure RTAQ. A similar

trend in the conductivity in such systems has been reported previously by different groups [25,26,61–65]. For composite 3, conductivity is least out of the three nanocomposites. Due to the higher concentration of nanoparticles and hence possibly due to aggregation, it is probable that small clumps of NPs disturbed the columnar structure of homeotropic alignment so there is no facile path for transportation of charges. Hence conductivity has not increased with the concentration of nanoparticles as expected. Earlier studies have also indicated this discrepancy [26,28,66].

Conductivity of composite 1 has been found to be $8.24 \times 10^{-8} \text{ S m}^{-1}$ in the isotropic phase. It increases with decrease in temperature, becoming $3.05 \times 10^{-7} \text{ S m}^{-1}$ at 80°C and finally reaching to $2.79 \times 10^{-6} \text{ S m}^{-1}$ at 28°C . The drastic increment in conductivity can be attributed to the ordered arrangement of discotic molecules and BTNPs as evidenced by the optical texture discussed in the previous section. Based on the Marcus equation, the theoretical description of the electron hopping rate between adjacent disks is explained by the transfer integral, which is a function of LUMO (or HOMO) orbitals of adjacent molecules for electron (or hole) transport and internal reorganization energy [67]. Charge transport in the bulk material depends on the degree of order within the columnar stack and thus on the overlap between the π orbitals [68]. Chandrasekhar *et al.* have asserted that the rigid core of DLCs is ordered, with the orientational order parameter S defined as

$$(S_D = \langle \frac{1}{2}(3\cos^2\theta - 1) \rangle), \quad (5)$$

where θ is the angle which the molecular symmetry axis makes with the director or column axis [69]. The core is not normal to the column axis but is inclined in columnar mesophases. It is established that the tilt of the molecular core persists in the columnar hexagonal phase as well [70]. Also, mobility depends more on the intracolumnar order than on the intercolumnar ordering [71]. Based on these facts, it can be inferred that the increase in the orientational order of rigid cores arises from the doping of BTNPs in the DLC matrix. The overlapping of the π orbitals of cores increases which in turn leads to increase in mobility along the columns. The BTNPs act as a conductive filler which bridges the defects within the columnar matrix [72]. Thus, high mobility along columns leads to high conductivity for composites (highest for composite 1). These experiments were repeated in order to validate the results obtained. X-ray diffraction studies discussed in the forthcoming section also explain increase of conductivity.

The inset of Fig. 7 shows the temperature dependence of ionic conductivity for pure RTAQ and composite 1 (for which conductivity is highest) during cooling from the isotropic phase. The increase in conductivity might be due to the hopping between localized sites involving both the BTNPs and the discoid aromatic cores. Also limiting the molecular rotation within the column leads to a decrease in the degree of freedom within the mesophase, and hence the charge carrier mobility of columns increases. It is important to mention that ionic conduction contributes to enhancement of total conductivity [12]. The inset also shows that with the decrease of temperature the formation of the column slowly improves and seems at the best at $\sim 50^\circ\text{C}$. This is point where conductivity

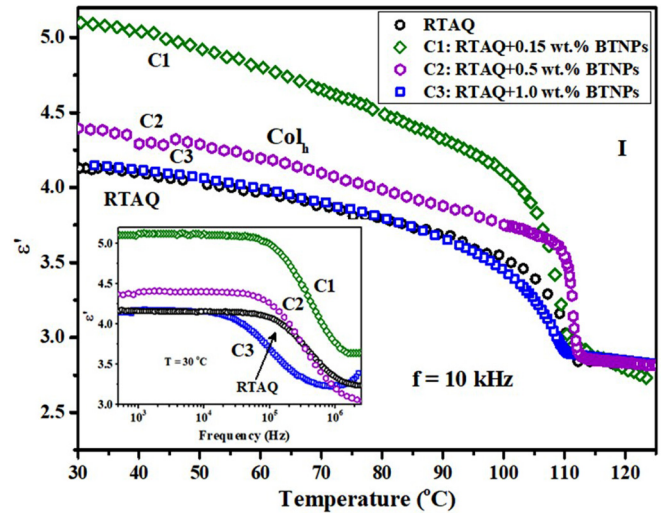


FIG. 8. Temperature dependence of permittivity (with normalized I-Col_h transition temperature and permittivity data) in the isotropic and Col_h phases for RTAQ and composites. Inset shows frequency dependence of the permittivity.

is highest and remains the same till room temperature. The highest value of the conductivity for composite 1 supports that column structures are best for this composition.

2. Frequency and temperature dependent permittivity

The temperature dependent static permittivity (ϵ') plots for pure RTAQ and its three composites (10 kHz) are shown in Fig. 8. All the plots show an abrupt jump in the value of the permittivity at the I-Col_h transition. Figure 8 shows that for pure RTAQ and composite 3, values of permittivity are almost same. But it has increased in composites 1 and 2 (highest in composite 1) as compared to pure RTAQ. As discussed in Sec. III A, the presence of BTNPs has a twofold effect. The first one is the dilution effect which decreases the number of LC molecules and hence their dipolar contribution (permittivity depends upon concentration of molecular dipoles). This caused reduction in the permittivity value say by $-\Delta\epsilon'_1$. The dilution effect increases with the increasing concentration of FNPs and hence magnitude of $\Delta\epsilon'_1$ increases. The second one is enhancement of the permittivity (say $\Delta\epsilon'_2$) due to the induction by ferroelectric BTNPs (see Fig. 5) which caused enhanced ordering as well as dipolar contribution. Thus total net change in the permittivity $\Delta\epsilon' = \Delta\epsilon'_2 - \Delta\epsilon'_1$. At certain critical doping concentration two interactions may counter each other resulting in net $\Delta\epsilon'$ being zero which is the case of composite 3. However, for low doping concentration (i.e., composites 1 and 2), the magnitude of $\Delta\epsilon'_1$ decreases and it is least for composite 1. Thus $\Delta\epsilon'$ is highest for composite 1 giving the highest increase in the permittivity with respect to pure RTAQ. One may counterargue that $\Delta\epsilon'_2$ will decrease with decreasing concentration of BTNPs. But in fact at high concentrations NPs start to show agglomeration (as discussed earlier) and therefore high concentration produces negative effect. Thus from these results, it is evident that composite 1 has optimum concentration of BTNPs to show enhancement of the

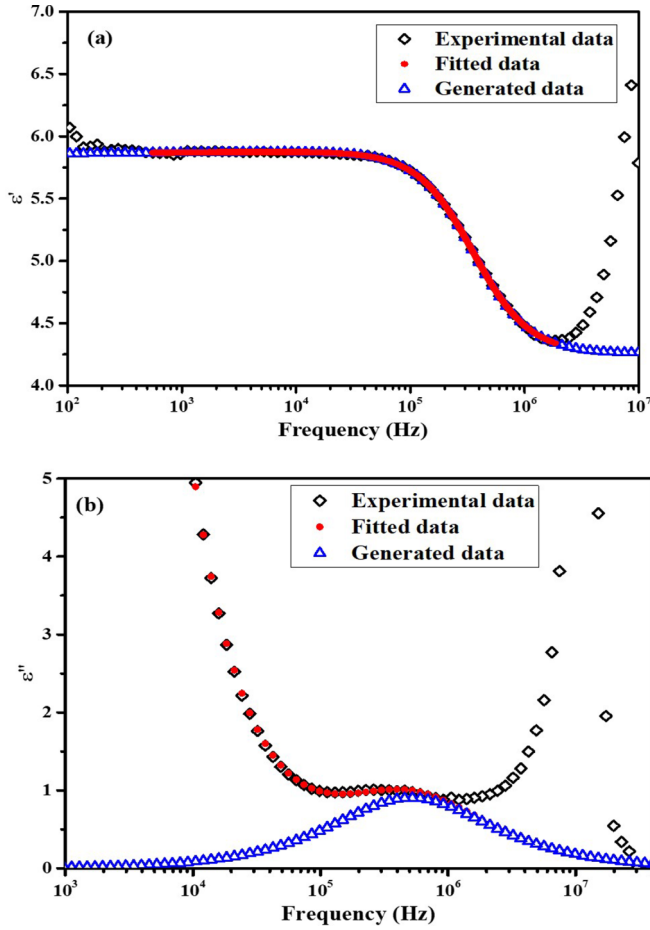


FIG. 9. Variation of (a) permittivity (ϵ'), and (b) loss (ϵ'') for composite 1 (RTAQ + 0.15 wt.% BTNPs) with frequency showing a relaxation phenomenon. Low and high frequency parasitic effects have been removed to find the actual relaxation plots shown by triangles.

permittivity. The same results are evident from conductivity measurement as discussed in previous paragraphs.

It is important to mention that thermodynamic results indicate that 0.5 wt.% of BTNPs in RTAQ (composite 2) is the optimum concentration for best stabilized columnar structure. However, dielectric results show that 0.15 wt.% of BTNPs in RTAQ (composite 1) shows the best results. In fact there is not too much difference between the results of composites 1 and 2. It seems that during the dielectric study, the presence of even small measuring voltage (electric field = $0.5 \text{ V}/10 \mu\text{m} = 50 \text{ kV/m}$) enhances the ferroelectric nature of BTNPs and further enhances $\Delta\epsilon'_2$. On the other hand due to the decreased number of BTNPs, the magnitude of $\Delta\epsilon'_1$ further decreases resulting increased in $\Delta\epsilon'$ ($=\Delta\epsilon'_2 - \Delta\epsilon'_1$). Thus dielectric parameters are best for composite 1.

At low temperatures, a slight decrement in ϵ' is seen for pure RTAQ as well as composites. This is due to lowering of relaxation frequency of a dispersion phenomenon observed above 10 kHz (see inset of Fig. 8). This effect is more prominent for the permittivity values at 100 kHz. The spectra for the permittivity (ϵ') and loss (ϵ'') for composite 1 are shown in Fig. 9. Beyond 10 kHz, a prominent dielectric relaxation

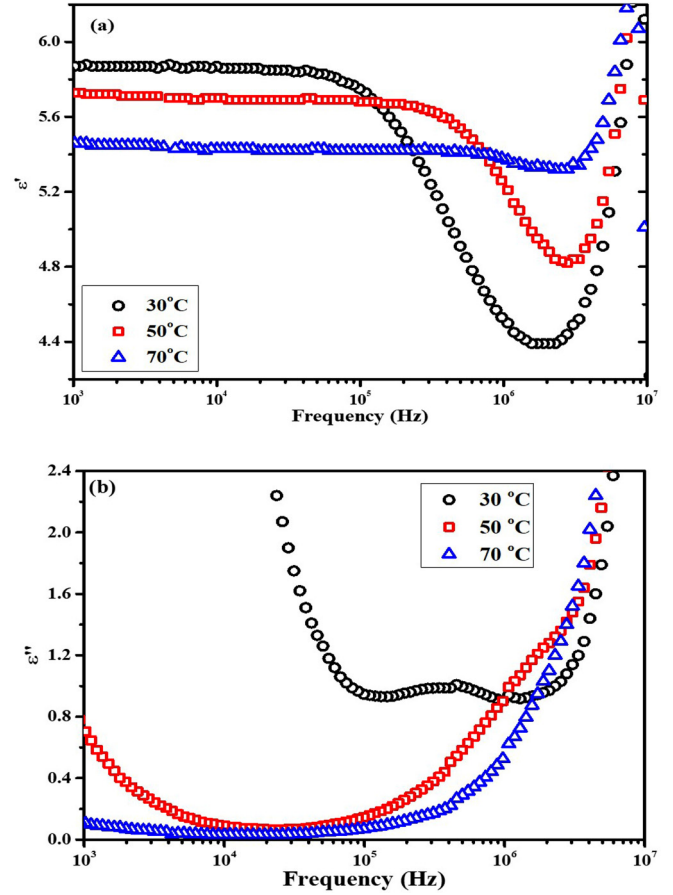


FIG. 10. Variation of (a) permittivity (ϵ'), and (b) loss (ϵ'') for composite 1 (RTAQ + 0.15 wt.% BTNPs) with frequency at different temperatures. As expected, with decrease of temperature, relaxation phenomenon shifts to low frequency side.

phenomenon can be seen in the Col_h phase (see Fig. 9). By the process of fitting of Eqs. (2) and (3) with the experimental data, low and high parasitic effects have been removed and the real relaxation mechanism free from artifacts is shown. The observed relaxation mechanism shifts to the low frequency region (see Fig. 10) with decrease in temperature. It happens due to increase in viscosity of the system with decrease of the temperature which ultimately slows down rotation of molecules under the measuring electric field. The dielectric spectra were fitted to the generalized Cole-Cole equations in order to calculate the relaxation frequencies and other dielectric parameters given in Table II. Dielectric parameters for pure RTAQ thus obtained agree with the literature reported earlier [73,74]. It has been observed that relaxation frequency (f_R) has marginally decreased in composite 1 as compared to RTAQ. This is due to the increased inertia of the system in the presence of BTNPs. The variation of relaxation frequency f_R with temperature (T) as shown in Fig. 11 follows the Arrhenius equation given as [28,38]

$$f_R = A \exp\left(\frac{-E_a}{RT}\right), \quad (6)$$

where E_a is the activation energy, R is the ideal gas constant, and T is the temperature. Using Eq. (6), the value of E_a for

TABLE II. Comparative table for permittivity (ϵ'), relaxation frequency (f_R in kHz), and distribution parameter (α) obtained from different methods, i.e., geometrically (α_{geom}) and fitting of Cole-Cole equations with experimental data (α_{calc}).

System	ϵ' (Col _h)		θ_{geom} (deg)	α_{geom} ($=2\theta_{\text{geom}}/\pi$) (rad)	α_{calc} (rad)	f_R (kHz)
	10 kHz	100 kHz				
RTAQ	4.17	4.05	9	0.10	0.03 ± 0.01	413 ± 4
RTAQ + 0.15 wt.% BTNPs	5.12	4.94	20	0.22	0.17 ± 0.02	357 ± 3

composite 1 is determined to be 38.5 kJ mol^{-1} . This is less than the value of E_a for pure RTAQ, which is 42.7 kJ mol^{-1} . The observed relaxation process is a Debye process since the value of the distribution parameter (α_i) has been found to be ~ 0 (see Table II), obtained by the procedure of fitting of experimental data as well as the Cole-Cole plots (see Fig. 12). Such type of relaxation mechanism has been observed in some other DLCs also. The relaxation process in pyrene derivatives displays relatively low values of activation energy in the range of 10 kJ mol^{-1} . This effect was attributed to localized fluctuations of the methylene groups [73,74]. The relaxation mode observed in pure RTAQ and the nanocomposites is due to the local fluctuations of peripheral chains surrounding the discotic mesogens [38]. An investigation of structural parameters of the Col_h phase of the doped samples will clear the picture in detail, as reported in the next section.

D. X-ray diffraction

Small angle x-ray scattering (SAXS) is a powerful tool for determining the nanoscale structure of matter [75]. SAXS is based on the detection of x-rays scattered by the sample at very low angles using dedicated instruments. It is applicable to any system exhibiting fluctuations in electron density, such as biopolymers in aqueous dispersions, nanoparticles in a solid or liquid matrix, or nanopores in a solid matrix. For a better understanding of the liquid crystalline phase of composite systems, spectra were recorded at different temperatures as

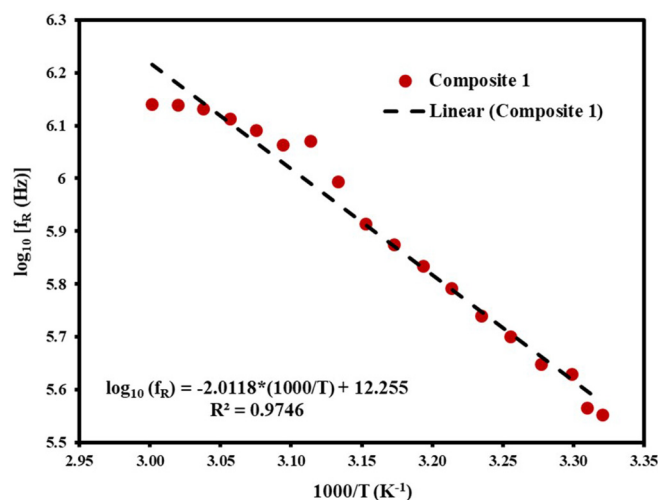


FIG. 11. Temperature dependence of relaxation frequency (f_R) with inverse of the temperature for composite 1 (RTAQ + 0.15 wt.% BTNPs) following Arrhenius behavior.

shown in Fig. 13. The SAXS profile of composite 1 shown in Fig. 13 is similar to those of composites 2 and 3 [38]. The profile shows two sharp peaks, one strong and the other weak reflection, in the small angle region. The d spacing of these two peaks is in the ratio $1:1/\sqrt{3}$ which is characteristic of a 2- d hexagonal lattice. These peaks are indexed as (10) and (11). The d spacing of the other two reflections is in the ratio $\frac{1}{2}:\frac{1}{\sqrt{7}}$ and they are indexed as the (20) and (21) peaks. These are also characteristic of a 2- d hexagonal lattice. Hence, the results clearly conclude that even after the inclusion of large sized nanoparticles, the 2- d Col_h lattice phase is not disrupted and is retained by the host molecules. In the wide-angle region, two peaks are observed: a broad background peak,

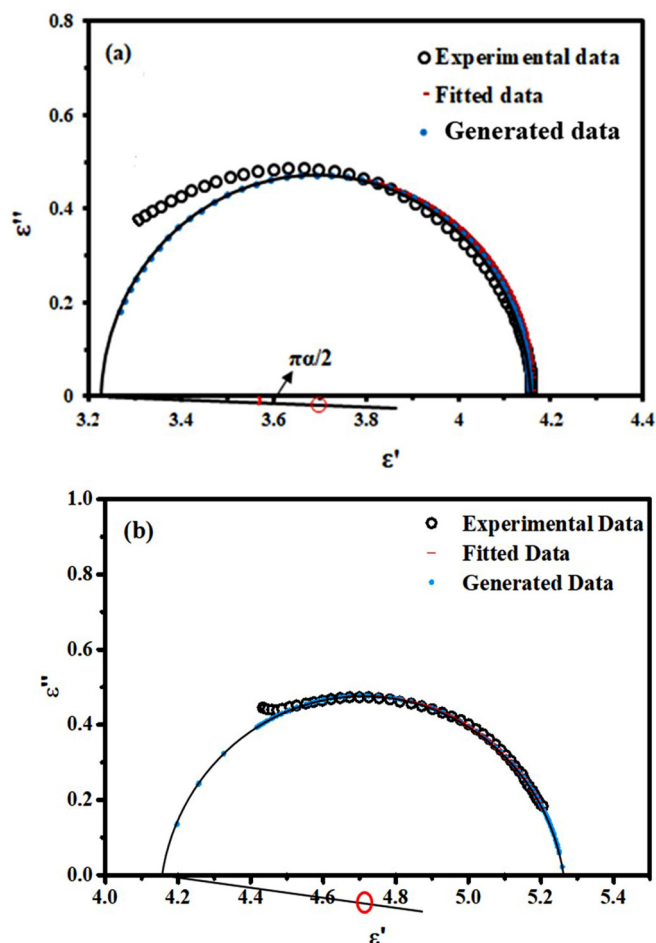


FIG. 12. Cole-Cole plots showing the variation of the loss with permittivity for (a) RTAQ and (b) composite 1 (RTAQ + 0.15 wt.% BTNPs).

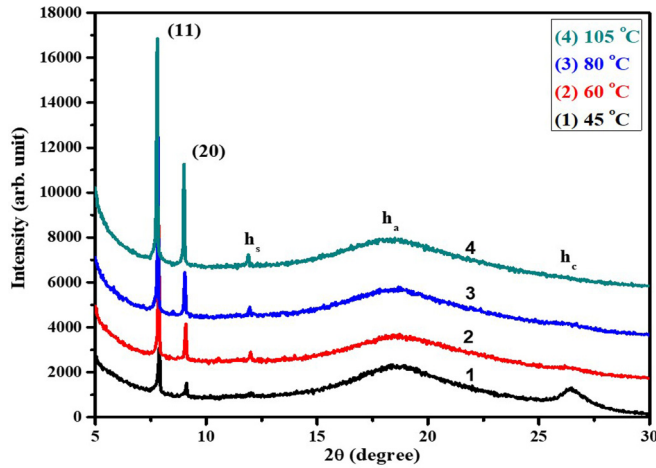


FIG. 13. X-ray diffraction spectra at different temperature for composite 1 (RTAQ + 0.15 wt.% BTNPs). Curves shifted vertically to enhance visibility.

i.e., the alkyl chain peak (h_a), and a sharp peak indicative of core-to-core (π - π) interaction (h_c). The h_a peak reflects the liquid-like correlation of the molten alkyl chains while the h_c peak corresponds to the separation between the discotic cores. h_c is indexed as (01) and is indicative of the columnar nature of the mesophase. h_a arises due to the interaction between the alkyl tails in the same column and suggests that the associated order is liquid-like. Similarly, the h_c peak appears because the molecular cores can pack better than the alkyl tails, which are in their molten state and hence occupy more volume [76]. Another sharp peak (h_s) in the middle-angle region appears because of the flip-flop arrangement of the compound inside the columns. The d spacing for the h_s peak is attributable to the weak correlation of the dyad along the normal to the disk plane (face-to-face correlation) and corresponds to the effective thickness of the folded dimer. Table III comprises

TABLE III. SAXS parameters, viz., layer spacing (d spacing in Å), intercolumnar distance (d_{inter} in Å), and average stacking distance ($d_{\text{core-core}}$ in Å) derived at different temperatures for RTAQ and composite 1 (RTAQ + 0.15 wt.% BTNPs).

System	T (°C)	d spacing (Å)	d_{inter} (Å)	$d_{\text{core-core}}$ (Å)
RTAQ	40 ^a	20.81	24.02	3.39
	25 ^b		22.40	3.43
RTAQ + 0.15 wt.% BTNPs	105	19.54	22.57	
	80	19.54	22.57	3.42
	60	19.44	22.45	3.40
	45	19.35	22.34	3.37
RTAQ + 0.5 wt.% BTNPs	45 ^c	19.33	22.32	3.36
RTAQ + 1.0 wt.% BTNPs	45 ^c	19.44	22.45	3.37

^aReference [65].

^bReference [33,57].

^cReference [38].

the d spacing, d -intercolumnar spacing, and d core-to-core separation values for composite 1 with respect to the decrease in temperature. A closer look at the ambient temperature values clearly confirms that d -intercolumnar spacing and d core-to-core separation have improved due to the insertion of nanoparticles. Large dopant size generates orientational defects locally, which destroys the colloidal homogeneity and lowers the orientational ordering in the matrix. Li *et al.* have estimated the critical particle size $R_{\text{max}} \sim \zeta = K/W$, the so-called surface extrapolation length being of the order of 100 nm, where K refers to the Frank constant, which typically equals 10^{-11} N, and W refers to coupling constant, which typically equals 10^{-4} J m⁻² [21]. Hence, the theory also supports our assumption for the existence of the Col_h phase in the doped system.

Table IV shows the variation of different lattice parameters associated with the hexagonal lattice and their correlations with respect to the decrease in temperature. The decrease in temperature signifies more pronounced formation of Col_h mesophases. This is because in the present case, the alignment of DLC molecules is temperature dependent. On comparing the values of d spacing and d core-to-core separation for the three nanocomposites, minima exist for composite 2 while maxima for composite 3. This supports our assumption that though the BTNP concentration is more in composite 2 as compared to composite 1, the formation and stability of columnar structure is best suited in composite 2. This could be only because of the fact that the ferroic nature of nanoparticles induces a local interaction field on the neighboring molecules and hence the LC ordering is enhanced. However, this effect is diminished in composite 3 with the addition of a large number of dopants which in turn increases the chances of agglomeration and hence disruption in the column formation. This result is similar to that discussed in the dielectric study. Table IV also shows the variation of lattice parameters a , b , and c associated with the Col_h phase. Commonly, for a hexagonal lattice, the relation between different lattice parameters is $a = b \neq c$, $\alpha = \beta = 90^\circ$, and $\gamma = 120^\circ$. The values of a , b , and c show a decrement with the temperature for composite 1. This might be because when the BTNPs try to accommodate inside the host matrix, the intercolumnar distance is affected minutely. The average stacking distance (separation between the cores of the mesogens) decreases due to the better overlapping of π orbitals. This facilitates a more efficient packing of the doped nanoparticles in the host matrix. This also explains the enhancement in the conductivity values for composite 1 at room temperature. Since hydrogen bonding plays a crucial role in the stacking of aromatic cores, the doped particles possibly have a greater affinity to bond with the substituent alkyl groups present around the rufigallol core.

Table IV also represents the correlation length of different lattice parameters for composite 1. Correlation distance (long-range order, distances between similar structures) is a measure of the phase size. This signifies the degree of order within the mesophases, calculated using the relation $\xi = (k2\pi)/(\Delta q)$, where k is the shape factor whose typical value is 0.89 and Δq is broadening in q (scattering vector) at half of the maximum intensity [77,78]. Δq is obtained by Lorentzian fitting of the diffraction pattern. Further, the correlation length of the peak was divided by the corresponding d spacing, which results

TABLE IV. Variation of d spacing (in Å), lattice parameters (i.e., plane indices or hk in Å), correlation lengths (ξ in Å), and corresponding number of correlated units [$\xi/(d$ spacing)] as obtained from SAXS measurements for composite 1 (RTAQ + 0.15 wt.% BTNPs) for the columnar hexagonal (Col_h) phase.

T (°C)	d spacing (Å)	Lattice parameters (Å)			Correlation length ξ (Å)		ξ/d_{spacing}	
		a, b	h_a	c	h_a	c	h_a	c
105	19.54	22.57	4.84		10.19		2.11	
80	19.54	22.57	4.80	3.42	10.95		2.28	
60	19.44	22.45	4.77	3.40	11.34		2.38	
45	19.35	22.34	4.75	3.37	14.09	60.54	2.97	17.96

in a measure for the spatial order in terms of dimensions of the molecular length scale [77,78]. This expresses the number of correlated units (n), i.e., signifies how many units of that length scale are *tuned in on* to show that correlation length. Since, for both the h_c and h_a peaks, the correlation length (ξ) is found to be more than 8, the phase can be assigned as discotic in nature [77,78]. The decrement in values with respect to decrease in temperature signifies that more rigid or ordered columnar packing is formed. A comparative analysis of ξ for all three composites signifies that a decrement in correlation values with increase in BTNP concentration for the h_a peak and increase in correlation values with increase in BTNP concentration for the h_c peak is observed. The above trend suggests that as the number of nanoparticles increases in the composite, more nanoparticles try to fit inside the columnar matrix. This increases the strain inside the matrix. Since h_a reflects the liquid-like correlation of the molten chains, the lower the number of nanoparticles, the more efficiently the alkyl chains occupy their position. Similarly, increase in correlation values with increase in dopant concentration for the h_c peak suggests that BTNPs in between the aromatic cores tends to strain the matrix and hence reduce the packing rigidity. However, this effect is compensated by the interactions between host and dopant molecules, as suggested by other parameters. Hence, a more efficient packing structure is formed for composite 2 as compared to composite 1. For composite 3, agglomeration supersedes all interactions and thus composite 2 shows the best suited results. Thus thermodynamic and SAXS results indicate that composite 2 possesses the most ordered columnar structure. However, dielectric and conductivity studies showed the best results for composite 1. In fact there is not too much difference between the results of composites 1 and 2 as discussed earlier. However, the presence of electric field during dielectric measurements enhanced ferroelectric properties of BTNPs and further enhanced the effective order of the system and hence related measured parameters for composite 1.

IV. CONCLUSION

A low concentration of ferroelectric barium titanate nanoparticles (BTNPs) dispersed in a room temperature discotic liquid crystal (DLC), namely 1,5-dihydroxy-2,3,6,7-

tetrakis(3,7-dimethyloctyloxy)-9,10-anthraquinone (RTAQ), has enhanced several physical parameters. We have observed that an optimum concentration of 0.5 wt.% of BTNPs in RTAQ has improved columnar structure as evidenced by small angle x-ray scattering (SAXS) studies. It has stabilized the mesomorphic state showing enhanced columnar (Col_h) to isotropic liquid phase transition temperature. Further lowering of BTNP concentration to 0.15 wt.% marginally decreases thermodynamic stability. However, conductivity has enhanced to $\sim 10^{-6} \text{ S m}^{-1}$ for 0.15 wt.% as compared to $10^{-11} \text{ S m}^{-1}$ for pure RTAQ; i.e., it has been enhanced by 5 orders of magnitude. Similarly, permittivity for the 0.15 wt.% system has increased by about 25% as compared to pure RTAQ. Enhancement of the conductivity and permittivity is highest for the composite having 0.15 wt.% of FNPs. Hence the composite having 0.15 wt.% of BTNPs has highly improved electrical characteristics at only marginal cost of thermodynamic stability (compared to the composite having 0.5 wt.% of BTNPs). Dielectric spectra has shown a low amplitude molecular relaxation mode at 413 kHz for RTAQ which shifts to 357 kHz for the composite having 0.15 wt.% of BTNPs. This decrease of the relaxation frequency is attributed to the increased inertia of the system due to the presence of BTNPs.

In concluding words, our experiments support that interaction of ferroelectric BTNPs with DLC molecules strengthened the order parameter and columnar structure of the Col_h phase and hence enhanced electrical properties for the low concentration of BTNPs. However, a higher concentration of these BTNPs in RTAQ proved to be destructive due to the agglomeration. Stabilization of the Col_h phase and enhancement of the various physical parameters proved that low concentration of ferroelectric NPs dispersed in room temperature RTAQ is useful for various applications, which includes one-dimensional conductors, organic photovoltaic cells, light emitting diodes, field effect transistors, and sensors.

ACKNOWLEDGMENTS

We wish to thank the Department of Science and Technology, Government of India, New Delhi, for financial support under FIST Grant No. SR/FST/PSI-216/2016. One of us (R.U.) thanks the University Grants Commission, New Delhi, for support through a University Research Fellowship.

[1] S. A. Maier, M. L. Brongersma, P. G. Kik, S. Meltzer, A. A. G. Requicha, and H. A. Atwater, *Adv. Mater.* **13**, 1501 (2001).

[2] J. N. Anker, W. P. Hall, O. Lyandres, N. C. Shah, J. Zhao, and R. P. V. Duyne, *Nat. Mater.* **7**, 442 (2008).

- [3] J. Oh, H. F. Gleeson, and I. Dierking, *Phys. Rev. E* **95**, 022703 (2017).
- [4] H. A. Atwater and A. Polman, *Nat. Mater.* **9**, 205 (2010).
- [5] M. J. Delaporte, E. J. Gałazka, P. M. Zielińska, and M. Marzec, *J. Mol. Liq.* **308**, 113039 (2020).
- [6] T. V. Bezrodna, G. V. Klishevich, N. D. Curmei, V. I. Melnyk, and V. V. Nesprava, *J. Appl. Spectrosc.* **84**, 560 (2017).
- [7] S. P. Yadav and S. Singh, *Prog. Mater. Sci.* **80**, 38 (2016).
- [8] Y. Shen and I. Dierking, *Appl. Sci.* **9**, 2512 (2019).
- [9] R. Basu and A. Garvey, *Appl. Phys. Lett.* **105**, 151905 (2014).
- [10] L. M. Lopatina and J. V. Selinger, *Phys. Rev. Lett.* **102**, 197802 (2009).
- [11] J. F. Blach, S. Saitzek, C. Legrand, L. Dupont, J. F. Henninor, and M. Warenghem, *J. Appl. Phys.* **107**, 074102 (2010).
- [12] A. Rudzki, D. R. Evans, G. Cook, and W. Haase, *Appl. Opt.* **52**, E6 (2013).
- [13] S. A. Basun, G. Cook, V. Y. Reshetnyak, A. V. Glushchenko, and D. R. Evans, *Phys. Rev. B* **84**, 024105 (2011).
- [14] J. G. An, S. Hina, Y. Yang, M. Xue, and Y. Liu, *Rev. Adv. Mater. Sci.* **44**, 398 (2016).
- [15] M. Mishra, S. Kumar, and R. Dhar, *Soft Mater.* **15**, 34 (2017).
- [16] P. Kopčanský, N. Tomašovičová, M. Koneracká, V. Závíšová, M. Timko, A. Džarová, A. Šprincová, N. Éber, K. F.-Csorba, T. T.-Katona, A. Vajda, and J. Jadzyn, *Phys. Rev. E* **78**, 011702 (2008).
- [17] A. Lorenz, N. Zimmermann, S. Kumar, D. R. Evans, G. Cook, M. F. Martinez, and H. S. Kitzerow, *J. Phys. Chem. B* **117**, 937 (2013).
- [18] R. K. Shukla, A. Chaudhary, A. Bubnov, V. Hamplova, and K. K. Raina, *Liq. Cryst.* **47**, 1379 (2020).
- [19] S. Y. Park and D. Stroud, *Phys. Rev. Lett.* **94**, 217401(2005).
- [20] S. P. Sreenilayam, D. Rodriguez-Lojo, V. P. Panov, V. Swaminathan, J. K. Vij, Yu. P. Panarin, E. Gorecka, A. Panov, and P. J. Stevenson, *Phys. Rev. E* **96**, 042701 (2017).
- [21] F. Li, O. Buchnev, C. I. Cheon, A. Glushchenko, V. Reshetnyak, Y. Reznikov, T. J. Sluckin, and J. L. West, *Phys. Rev. Lett.* **97**, 147801 (2006); **99**, 219901(E) (2007).
- [22] Supreet, S. Kumar, K. K. Raina, and R. Pratibha, *Liq. Cryst.* **40**, 228 (2013).
- [23] C. Kavitha, B. S. Avinash, S. Kumar, and V. Lakshminarayanan, *Mater. Chem. Phys.* **133**, 635 (2012).
- [24] S. Eustis and M. A. El-Sayed, *Chem. Soc. Rev.* **35**, 209 (2006).
- [25] S. Kumar and V. Lakshminarayanan, *Chem. Commun.* **14**, 1600 (2004).
- [26] L. A. Holt, R. J. Bushby, S. D. Evans, A. Burgess, and G. A. Seeley, *J. Appl. Phys.* **103**, 063712 (2008).
- [27] S. Lalik, A. Deptuch, T. J. Gołab, P. Fryń, D. Dardas, O. Stefańczyk, M. Urbańska, and M. Marzec, *J. Phys. Chem. B* **124**, 6055 (2020).
- [28] N. Yadav, S. Kumar, and R. Dhar, *RSC Adv.* **5**, 78823 (2015).
- [29] B. Jaffe, W. R. Cook Jr., and H. Jaffe, *Piezoelectric Ceramics* (Academic Press, London, 1971).
- [30] A. R. Imamaliyev, M. A. Ramazanov, and S. A. Humbatov, *Beilstein J. Nanotechnol.* **9**, 824 (2018).
- [31] H. Zhang, *AIP Adv.* **3**, 042118 (2013).
- [32] M. Acosta, N. Novak, V. Rajas, S. Patel, R. Vaish, J. Koruza, G. A. Rozsetti Jr., and J. Rodel, *Appl. Phys. Rev.* **4**, 041305 (2017).
- [33] H. K. Bisoyi and S. Kumar, *Tetrahedron Lett.* **48**, 4399 (2007).
- [34] S. Tsunekawa, S. Ito, T. Mori, K. Ishikawa, Z. Q. Li, and Y. Kawazoe, *Phys. Rev. B* **62**, 3065 (2000).
- [35] T. Yu, Z. X. Shen, W. S. Toh, J. M. Xue, and J. Wang, *J. Appl. Phys.* **94**, 618 (2003).
- [36] S. A. Zangana, M. Turner, and I. Dierking, *J. Appl. Phys.* **121**, 085105 (2017).
- [37] M. Tanaka and Y. Makino, *Ferroelectr. Lett. Sect.* **24**, 13 (1998).
- [38] R. Uttam, N. Yadav, S. Kumar, and R. Dhar, *J. Mol. Liq.* **294**, 111609 (2019).
- [39] K. S. Cole and R. H. Cole, *J. Chem. Phys.* **9**, 341 (1941).
- [40] S. L. Srivastava and R. Dhar, *Indian J. Pure Appl. Phys.* **29**, 745 (1991).
- [41] R. Dhar, *Indian J. Pure Appl. Phys.* **42**, 56 (2004).
- [42] R. Dhar, R. S. Pandey, and V. K. Agrawal, *Indian J. Pure Appl. Phys.* **40**, 901 (2002).
- [43] M. V. Gorkunov and M. A. Osipov, *Soft Matter* **7**, 4348 (2011).
- [44] M. Mishra, R. S. Dabrowski, and R. Dhar, *J. Mol. Liq.* **213**, 247 (2016).
- [45] T. D. Ibragimov, A. R. Imamaliyev, and G. M. Bayramov, *Ferroelectrics* **495**, 60 (2016).
- [46] X. Feng, L. S. Vargas, S. Umadevi, T. Mori, Y. Shimizu, and T. Hegmann, *Adv. Func. Mater.* **25**, 1180 (2015).
- [47] S. Kumar, S. K. Pal, and V. Lakshminarayanan, *Mol. Cryst. Liq. Cryst.* **434**, 251 (2005).
- [48] M. Gupta, I. Satpathy, A. Roy, and R. Pratibha, *J. Coll. Inter. Sci.* **352**, 292 (2010).
- [49] M. V. Gorkunov, G. A. Shandryuk, A. M. Shatalova, I. V. Kutergina, A. S. Merekolov, Y. Kudryavtsev, R. V. Tolroze, and M. A. Osipov, *Soft Matter* **9**, 3578 (2013).
- [50] Y. Reznikov, O. Buchnev, O. Tereshchenko, V. Reshetnyak, A. Glushchenko, and J. West, *Appl. Phys. Lett.* **82**, 1917 (2003).
- [51] M. Mishra, S. Kumar, and R. Dhar, *Thermochim. Acta* **631**, 59 (2016).
- [52] A. S. Pandey, R. Dhar, S. Kumar, and R. Dabrowski, *Liq. Cryst.* **38**, 115 (2011).
- [53] S. H. Eichhorn, A. Adavelli, H. S. Li, and N. Fox, *Mol. Cryst. Liq. Cryst.* **397**, 47 (2003).
- [54] P. Oswalt, F. Melo, and C. Germain, *J. Phys. I* **50**, 3527 (1989).
- [55] T. Brunet, O. Theibaut, E. Charlet, and H. Bock, *Europhys. Lett.* **93**, 16004 (2011).
- [56] S. Kumar, *Liq. Cryst. Today* **18**, 2 (2009).
- [57] H. K. Bisoyi and S. Kumar, *New J. Chem.* **32**, 1974 (2008).
- [58] M. Kumar and S. Kumar, *RSC Adv.* **5**, 1262 (2015).
- [59] A. K. Jonscher, *Nature (London)* **267**, 673 (1977).
- [60] S. L. Srivastava and R. Dhar, *Radiat. Phys. Chem.* **47**, 287 (1996).
- [61] S. Kumar, S. K. Pal, P. S. Kumar, and V. Lakshminarayanan, *Soft Matter* **3**, 896 (2007).
- [62] A. N. Gowda, M. Kumar, A. R. Thomas, R. Philip, and S. Kumar, *ChemSelect* **1**, 1361 (2016).
- [63] N. Boden, R. J. Bushby, and J. Clements, *J. Chem. Phys.* **98**, 5920 (1993).
- [64] V. S. K. Balagurusamy, S. K. Prasad, S. Chandrasekhar, S. Kumar, and C. V. Yelamaggad, *Pramana* **53**, 3 (1999).
- [65] S. Varshney, M. Kumar, A. Gowda, and S. Kumar, *J. Mol. Liq.* **238**, 290 (2017).
- [66] K. K. Vardanyan, R. D. Walton, D. M. Sita, I. S. Gurfinkiel, and W. M. Saidel, *Liq. Cryst.* **39**, 595 (2012).

- [67] V. Lemaur, D. A. da Silva Filho, V. Coropceanu, M. Lehmann, Y. Geerts, J. Piris, M. G. Debije, A. M. van de Craats, K. Senthilkumar, L. D. A. Siebbeles, J. M. Warman, J. L. Bredas, and J. Cornil, *J. Am. Chem. Soc.* **126**, 3271 (2004).
- [68] M. Lehmann, G. Kestemont, R. G. Aspe, C. B. Herman, M. H. J. Koch, M. G. Debije, J. Piris, M. P. de Haas, J. M. Warman, M. D. Watson, V. Lemaur, J. Cornil, Y. H. Geerts, R. Gearba, and D. A. Ivanov, *Chem. Eur. J.* **11**, 3349 (2005).
- [69] S. Chandrasekhar and G. S. Ranganath, *Rep. Prog. Phys.* **53**, 57 (1990).
- [70] M. Yoneya, T. Makabe, A. Miyamoto, Y. Shimizu, Y. Miyake, H. Yoshida, A. Fujii, and M. Ozaki, *Phys. Rev. E* **89**, 062505 (2014).
- [71] A. M. van de Craats, J. M. Warman, A. Fechtenkötter, J. D. Brand, M. A. Harbison, and K. Mullen, *Adv. Mater.* **11**, 1469 (1999).
- [72] T. A. Wood, J. S. Lintuvuori, A. B. Schofield, D. Marenduzzo, and W. C. K. Poon, *Science* **334**, 79 (2011).
- [73] C. Krause, H. Yin, C. Cerclier, D. Morineau, A. Wurm, C. Schick, F. Emmerling, and A. Schönhals, *Soft Matter* **8**, 11115 (2012).
- [74] S. Calus, A. V. Kityk, L. Borowik, R. Lefort, D. Morineau, C. Krause, A. Schönhals, M. Busch, and P. Huber, *Phys. Rev. E* **92**, 012503 (2015).
- [75] O. Glatter and O. Kratky, *Small Angle X-Ray Scattering* (Academic Press, New York, 1982).
- [76] S. K. Prasad, D. S. S. Rao, S. Chandrasekhar, and S. Kumar, *Mol. Cryst. Liq. Cryst.* **396**, 121 (2003).
- [77] M. Gupta, S. P. Gupta, M. V. Rasna, D. Adhikari, S. Dhara, and S. K. Pal, *Chem. Commun.* **53**, 3014 (2017).
- [78] J. De, S. P. Gupta, I. Bala, S. Kumar, and S. K. Pal, *Langmuir* **33**, 13849 (2017).